Auto-associative heparin nanoassemblies: A biomimetic platform against the heparan sulfate-dependent viruses HSV-1, HSV-2, HPV-16 and RSV

UNIVERSITÀ DEGLI STUDI DI TORINO

Auto-associative heparin nanoassemblies: a biomimetic platform against the heparan-sulfate-dependent viruses HSV-1, HSV-2, HPV-16 and RSV

David LEMBO[a], Manuela DONALISIO[a], Claire LAINE[b], Valeria CAGNO[a], Andrea CIVRA[a], Elsa P. BIANCHINI[c], Narimane ZEGHBIB[b], Kawthar BOUCHEMAL[b*]

[a] University of Turin, Department of Clinical and Biological Sciences, Regione Gonzole 10, 10043 Torino, Italy

[b] Univ Paris-Sud, Institut Galien Paris Sud, UMR CNRS 8612, Faculté de Pharmacie, 5, rue J.B. Clément, 92296 Châtenay-Malabry cedex, France

[c] Univ Paris Sud, Laboratoire d'hématologie, Faculté de Pharmacie, 5, rue J.B. Clément, 92296 Châtenay-Malabry cedex, France.

*Corresponding author:

Kawthar BOUCHEMAL,

PhD. Associate Professor. Institut Galien Paris Sud, UMR CNRS 8612, University Paris-Sud, Faculty of Pharmacy. 5, Rue J.B. Clément. 92296 Châtenay-Malabry cedex, France.

Fax : +33 (0)1 46 61 93 34.

e-mail : kawthar.bouchemal@u-psud.fr

Abstract

A new, simple and green method was developed for the manufacturing of heparin nanoassemblies active against the heparan-sulfate-dependent viruses HSV-1, HSV-2, HPV-16 and RSV. These nanoassemblies were obtained by the auto-association of *O*-palmitoyl-heparin and α-cyclodextrin in water. The synthesized *O*-palmitoyl-heparin derivatives mixed with α-cyclodextrin resulted in the formation of crystalline hexagonal nanoassemblies as observed by transmission electron microscopy. The nanoassembly mean hydrodynamic diameters were modulated from 340 to 659 nm depending on the type and the initial concentration of *O*-palmitoyl-heparin or α-cyclodextrin. The antiviral activity of the nanoassemblies was not affected by the concentration of the components. However, the method of the synthesis of *O*-palmitoyl-heparin affected the antiviral activity of the formulations. We showed that reduced antiviral activity is correlated to lower sulfation degree and anticoagulant activity.

Keywords: Nanoassemblies, α-cyclodextrin, glycosaminoglycan, HSV, HPV, heparin.

1. Introduction

The first step in the infection of mucosal surfaces by viruses involves their attachment to cellular receptors exposed on the surface of epithelial cells. In many instances, virus–cell interaction is mediated by cell surface heparan sulfate proteoglycans (HSPGs) [1,2]. These negatively charged molecules are a core protein linked to glycosaminoglycan (GAG) chains of unbranched sulfated polysaccharides known as heparan sulfates (HS). HS are structurally related to heparin except that heparin has higher level of sulfation and higher content of iduronic acid [3,4].

The interaction between the viruses and HSPGs occurs between the basic amino acid residues of viral proteins and the negatively charged sulfated/carboxyl groups of the GAG chains. For this reason heparin and other GAGs can competitively interfere with virus attachment to cells. Many viruses exploit HSPGs as attachment receptors, namely the herpes simplex virus type 1 and type 2 (HSV-1 and HSV-2), the human papilloma virus (HPV) and respiratory ysyncytial virus (RSV) [5-7].

So far, GAGs have been explored as potential candidate in the prevention of viral infections [8,9]. Accumulated data from the literature indicates that the inhibitory effect of heparin and HS was demonstrated on HSV by acting on its earliest phase [10,11], while the binding of HPV-like particles to cells has been shown to be inhibited by heparin [12]. HS has proved to play an important role in the prevention of HPV infections [13].

Surprisingly, although numerous research works were already described in the literature on the activity of GAGs against viral mucosal infections, there is a clear gap concerning the design of efficient locally-administrated formulations. Besides the prevention of the infection, the formulation of GAGs as a drug delivery system able to target the viruses, to load antiviral drugs

and to control their release over time represents an interesting strategy against viral mucosal infections. However, although the large number of publications in the field of drug delivery systems, current nanotechnologies have, unfortunately, important limitations due to the complexity of the processes used to their manufacturing and thus the difficulty for the scaling-up of their production to pharmaceutical companies. Furthermore, manufacture processes require the use of toxic solvents (acetone and ethanol for flash nanoprecipitation), surfactants, polymerization initiators and extremely reactive monomers (anionic and radical emulsion polymerization). Expensive techniques must be employed to completely remove the solvents and the surfactants at the end of the preparation process. Solvent and surfactant traces may persist and constitute a drawback for the medical applications of these systems. While monomers present in the polymerization medium could interact with the drug leading to its instability and the formation of toxic products.

In this context, Bouchemal's group has designed an innovative drug delivery system composed of nanoassemblies spontaneously formed in aqueous medium without using surfactants, pH modification and without heating or purification steps [14]. In this process, nanoassemblies were obtained by mixing a hydrophobically-modified polysaccharide and an α-cyclodextrin (α-CD).

The aim of the present work is to use this process to obtain new GAG-based nanoassemblies and to evaluate their ability to inhibit viral attachment to cells. We took advantage of structural similarities between heparin and cell surface HS and evaluated the antiviral activity of heparin-based formulations. The preparation of heparin nanoassemblies was achieved by the self-association in aqueous media of *O*-palmitoyl-heparin (OPH) and α-CD. This biomimetic barrier could act like a "trap" able to specifically catch up the viruses and avoid their attachment to the cells. The effect of the chemical modification of OPH on the antiviral activity was evaluated

against HSV-1, HSV-2, RSV and the high-risk type of HPV (HPV-16) involved in cervical cancers. Rotavirus, a HSPG-independent virus was used as control.

2. Materials

Heparin sodium salt from porcine intestinal mucosa 500 kU, palmitoyl chloride, anhydrous pyridine, sodium chloride and sodium acetate were from Sigma (Saint-Quentin Fallavier, France). Acetone was from Carlo Erba (Val de Reuil, France). α-CD was from Cyclolab (Budapest, Hungary). Anhydrous dimethylformamide (DMF), anhydrous dichloromethane (DCM), diethylether, ethanol, methanol were from VWR (Fontenay sous-bois, France).

Cells. African green monkey fibroblastoid kidney cells (Vero) (ATCC CCL-81) , human epithelial cells Hep-2 (ATCC CCL-23), A549 (ATCC CCL-185) and african green monkey kidney epithelial (MA-104) cells (ATCC CRL-2378.1) were grown as monolayers in Eagle's minimal essential medium (MEM) (Gibco/BRL, Gaithersburg, MD) supplemented with 10 % heat inactivated fetal calf serum and 1 % antibiotic-antimycotic solution (Zell Shield, Minerva Biolabs GmbH, Berlin, Germany). The 293TT cell line, derived from human embryonic kidney cells transformed with the simian virus 40 (SV40) large T antigen, was cultured in Dulbecco's modified Eagle's medium (DMEM) (Gibco-BRL, Gaithersburg, MD) supplemented with heat-inactivated 10 % fetal calf serum (FCS; Gibco- BRL), Glutamax-I 1 % (Invitrogen, Carlsbad, CA) and nonessential amino acids 1 % (Sigma Aldrich, Steinheim, Germany). 293TT cells allow high levels of protein to be expressed from vectors containing the SV40 origin due to over replication of the expression plasmid [15].

Viruses. Clinical isolates of HSV-1 and HSV-2 were kindly provided by Prof. M. Pistello, University of Pisa, Italy. HSV-1 and HSV-2 strains were propagated and titrated by plaque assay on Vero cells. RSV strain A2 (ATCC VR-1540) was propagated in Hep-2 and titrated by the

indirect immunoperoxidase staining procedure using an RSV monoclonal antibody (Ab35958; Abcam, Cambridge, United Kingdom) as described previously [16]. Human rotavirus strain Wa (ATCC VR-2018) was activated with 5 µg/mL of porcine pancreatic trypsin type IX (Sigma, St. Louis, Mo.) for 30 minutes at 37 °C and propagated in MA104 cells by using MEM containing 0.5 µg of trypsin per mL as described previously [17]. Virus stocks were maintained frozen (-80 °C).

HPV PsV production. Plasmids and 293TT cells used for pseudovirus (PsV) production were kindly provided by John Schiller (National Cancer Institute, Bethesda, MD). Detailed protocols and plasmid maps for this study can be seen at http://home.ccr.cancer.gov/lco/default.asp. HPV16 PsVs were produced according to previously described methods [18]. Briefly, 293TT cells were transfected with a plasmid, named p16LLw, expressing the papillomavirus major and minor capsid proteins (L1 and L2, respectively), together with a reporter plasmid expressing the secreted alkaline phosphatase (SEAP), named pYSEAP. Capsids were allowed to mature overnight in cell lysate; the clarified supernatant was then loaded on top of a density gradient of 27 to 33 to 39 % Optiprep (Sigma-Aldrich, St. Louis, MO) at room temperature for 3 h. The material was centrifuged at 28000 rpm for 16 h at 4 °C in an SW41.1 rotor (Beckman Coulter, Inc., Fullerton, CA) and then collected by bottom puncture of the tubes. Fractions were inspected for purity in 10% sodium dodecyl sulfate (SDS)–Tris–glycine gels, titrated on 293TT cells to test for infectivity by SEAP detection, and then pooled and frozen at -80 °C until needed. The L1 protein content of PsV stocks was determined by comparison with bovine serum albumin standards in Coomassie-stained SDS-polyacrylamide gels.

3. Methods

3.1. Preparation of *O*-palmitoyl heparin.

Two methods for the esterification of heparin were used:

Method 1. Synthesis of OPH-1: Heparin (1 g) was suspended into 11 mL of anhydrous DCM and heated at 60 °C under magnetic stirring. Then, anhydrous pyridine (5 mL) was added followed by palmitoyl chloride (2.5 g) dissolved in 6 mL anhydrous DMF under continuous magnetic stirring at 60 °C during 2 h and 1 h at room temperature. Then, 100 mL of cold ethanol (at 4 °C) was added. The precipitate was collected and washed with 100 mL of ethanol, then with 100 mL of diethylether using a Buchner filter. The solid materials were dried under vacuum at room temperature.

Method 2. Synthesis of OPH-2: Heparin (2 g) was added to 10 mL of anhydrous DCM and palmitoyl chloride (2.5 g) under continuous magnetic stirring at room temperature during 72 h. Then, 20 mL of a solution of 10 % of sodium acetate in methanol was added. The precipitate was collected and washed with 100 mL of methanol then with 100 mL of acetone using a Buchner filter. The solid materials were dried under vacuum at room temperature. The ester was then purified by dissolution in 10 mL of water and progressive addition of NaCl until the concentration reaches 10 %. After the addition of 20 mL of methanol, the precipitate formed was collected and washed with methanol and acetone and dried under vacuum at room temperature.

3.2. Chemical characterization of *O*-palmitoyl heparin.

The synthesized heparins were then characterized by using Attenuated total reflectance-Fourier transform infrared (ATR-FTIR) spectroscopy. Infrared spectra were obtained with an ATR-IR spectrometer (FT/IR-

4100, JASCO) operating at 4 cm^{-1} resolution. Fifty scans were accumulated in each run and referred to air. The ATR sampling device utilized a diamond internal reflection element embedded into a ZnSe support/focusing element in a single reflection configuration. The resultant spectra over the range of 4000–400 cm^{-1} was analyzed using the IR Protein Secondary Structure Analysis program (JASCO Co).

The total amount of carbon and sulfur in esterified heparins and native heparin was determined by elemental analysis using an Analyzer LECO SC144 (Service central d'analyse du CNRS, Vernaison, France). Samples of 20 mg were burned at 1350 °C over oxygen flux and the detection of SO_2 was performed by infrared measurements.

The degree of substitution of each derivative was evaluated from the determination of the percentage of carbon in comparison with native heparin.

$$DS = \left(\frac{C\%}{6}\right)_{OPH} - \left(\frac{C\%}{6}\right)_{Heparin} \quad \text{Eq.1}$$

2.3. Preparation and physico-chemical characterization of nanoassemblies

Preparation of the nanoassemblies. Nanoassembly suspensions were prepared by mixing a suspension of OPH and a solution of α-CD at room temperature under magnetic stirring during 72 h. The effect of the variation of each component on the size of the nanoassemblies was then studied.

Size measurements. The hydrodynamic diameter of the nanoassemblies was determined at 25 °C by quasi-elastic light scattering using a Zetasizer Nanoseries Nano-ZS (Malvern Instruments, France). The scattered angle was fixed at 173° and 30 µL of each sample was diluted in 1 mL of MilliQ® water.

166 *Zeta potential determination*.

167 Zeta potential of nanoassemblies was measured using Zetasizer Nanoseries (Malvern Instruments
168 Ltd. UK). The dilution of the suspensions (1:33 (v/v)) was performed in NaCl (1 mM). Each
169 experiment was replicated three times.

170 *Transmission Electron Microscopy.* The TEM images were obtained using the transmission
171 electron microscope of 60 kV Jeol 1400 (Imagif, Gif sur Yvette, France). For this, 1 µL of the
172 nanoassembly suspension was diluted in 29 µL of MilliQ® water. Then, 3 µL of this dilution are
173 placed on a grid. After 5 minutes of drying, the grid is inserted into the microscope to view the
174 sample.

175 2.4. Anticoagulant activity evaluation. The anticoagulant activity of the
176 nanoassemblies was in vitro evaluated by the measurement of anti-Xa activity with the Sta-
177 Rotachrom Heparin assay (Diagnostica-Stago) in a pool of normal human plasma provided by
178 Cryocheck company. Plasma will be supplemented with the nanoassemblies, and after 5 minutes,
179 anti-FXa activity was measured following the manufacturer's recommendations. The results were
180 compared to the native heparin [19].

181 2.5. Cell viability assay. Cell viability was measured by the MTS [3-(4,5-dimethylthiazol-
182 2-yl)-5-(3-carboxymethoxyphenyl)-2-(4-sulfophenyl)-2H-tetrazolium] assay. Confluent cell
183 cultures seeded in 96-well plates were incubated with different concentrations of nanoassemblies
184 (calculated on the heparin content) in triplicate under the same experimental conditions described
185 for the antiviral assays. Cell viability was determined by the CellTiter 96 Proliferation Assay Kit
186 (Promega, Madison, WI,USA) according to the manufacturer's instructions. Absorbances were
187 measured using a Microplate Reader (Model 680, BIORAD) at 490 nm. The effect on cell
188 viability at different concentrations of nanoassemblies was expressed as a percentage, by

189 comparing absorbances of treated cells with the ones of cells incubated with culture medium
190 alone. The 50 % cytotoxic concentrations (CC_{50}) and 95 % confidence intervals (CIs) were
191 determined using Prism software (Graph-Pad Software, San Diego, CA).

192 2.6. In vitro antiviral assays

193 *HSV inhibition assays.* The effect of nanoassemblies on HSV infection was evaluated by a plaque
194 reduction assay. Vero cells were preplated 24 h in advance in 24-well plates at a density of 10 x
195 10^4 cells. Increasing concentrations of nanoassemblies (calculated on the heparin content) were
196 incubated with HSV-1 or HSV-2 (MOI 0.0003 pfu/cell) at 37 °C for one hour and then the
197 mixtures were added to cells. Following virus adsorption (2 h at 37 °C), the virus inoculum was
198 removed, the cells were washed and then overlaid with a medium containing 1.2 %
199 methylcellulose (Sigma). After 24 h (HSV-2) or 48 h (HSV-1) of incubation at 37 °C, cells were
200 fixed and stained with 0.1 % crystal violet in 20 % ethanol and viral plaques were counted. The
201 concentration producing 50 % reduction in plaque formation (IC_{50}) was determined using the
202 Prism software by comparing drug-treated and untreated wells.

203 *HPV inhibition assays.* 293TT cells were preplated 24 h in advance in 96-well tissue culture-
204 treated flat bottom plates at a density of 20000 cells/well in 100 µL of neutralization buffer
205 (DMEM without phenol red, 10 % heat-inactivated fetal bovine serum, 1 % glutamate, 1 %
206 nonessential aminoacids, 1 % penicillin-streptomycin-fungizone, and 10 mM HEPES). Diluted
207 PsV stocks (80 µL/well) were placed on 96-well non treated sterile, polystyrene plates (Nalge-
208 Nunc, Roskilde, Denmark), combined with 20 µL of serially diluted nanoassemblies, and placed
209 for 1 h at 37°C. The 100-µL PsV-compound mixture was transferred onto the preplated cells and
210 incubated for 72 h. The final concentration of PsV was approximately 1 ng/mL L1. After
211 incubation, 25 µL of supernatant was harvested. The SEAP content in the supernatant was

212 determined using a Great Escape SEAP Chemiluminescence Kit (BD Clon- tech, Mountain View,
213 CA) as directed by the manufacturer.

214 *RSV inhibition assay.* Nanoassemblies were serially diluted and incubated with virus (MOI 0.01)
215 for one hour at 37 °C. Then the mixture was added to A549 cells grown as monolayers in a 96-
216 well plate to allow the viral adsorption for 3 h at room temperature; the monolayers were then
217 washed and overlaid with 1.2 % methylcellulose medium. Three days post-infection, cells were
218 fixed with cold methanol and acetone for 1 min and subjected to RSV-specific immunostaining.
219 Immunostained plaques were counted, and the percent inhibition of virus infectivity was
220 determined by comparing the number of plaques in treated wells with the number in untreated
221 control wells.

222 *Rotavirus inhibition assay.* Assays of inhibition of rotavirus infectivity were carried out with
223 confluent MA104 cell monolayers plated in 96-well trays. Virus infectivity was activated with
224 5 μg of porcine trypsin (Sigma)/mL for 30 minutes at 37 °C. Activated virus (MOI 0.02 pfu/cell)
225 was incubated for one hour at 37 °C in presence of different concentrations of nanoassemblies.
226 The virus-nanoassembly mixtures were added on cells for one hour at 37 °C and then the cells
227 were washed and fresh medium was added. After 16 h, cells were fixed with cold acetone-
228 methanol (50:50), and viral titers were determined by indirect immunostaining by using the
229 monoclonal antibody mab0036 (specific for human 41 kDa inner capsid protein - VP6 - of
230 Rotavirus) purchased from Covalab (Villeurbanne, France) and the UltraTech HRP Streptavidin-
231 Biotin Detection System (Beckman Coulter).

232 **Data analysis.** All results are presented as the mean values from three independent experiments.
233 The IC50 values for inhibition curves were calculated by regression analysis using the program
234 GraphPad Prism version 4.0 (GraphPad Software, San Diego, California, U.S.A.) to fit a variable

slope-sigmoidal dose–response curve. A selectivity index (SI) was calculated by dividing the CC_{50} by the IC_{50} value.

3. Results and discussion

The heparan-sulfate dependent viruses HSV-1, HSV-2, HPV-16 and RSV interact with HSPGs receptors on the epithelial cells facilitating thus their initial attachment and subsequent cellular entry and infection. In the present work a new approach was proposed to design locally-administrated HS-mimetic formulations able to specifically target the viruses and avoid their attachment to the mucosal surfaces. HS is distinguished from the closely related GAG heparin by its lower degree of sulfation, higher degree of *N*-acetylation compared with the *N*-sulfation of glucosamine residues, and the predominance of glucuronic acid rather than iduronic acid [20]. Taking advantage of the similarities between heparin and HS, heparin was used in this work as a GAG model for investigating the ability of heparin nanoassemblies to inhibit HS-dependent viruses. Heparin nanoassemblies were obtained by a new, simple and green method based on the self-association of heparin grafted with palmitic acid residues and α-CD in water without using surfactants, pH modification and without heating or purification steps.

O-palmitoyl-heparin was obtained using two different methods as indicated in Figure 1. ATR-IR spectroscopy was used to reveal the grafting of palmitic acid on heparin (Figure 2). In comparison with native heparin, the spectrum of OPH-1 showed two additional small peaks at 2929 cm^{-1} and 1733 cm^{-1}. The first band was attributed to the stretching vibrations of C-H bounds of $–CH_2–$ and $–CH_3$ groups of palmitic acid grafted on OPH-1, while the second band was due to ester function.

The presence of alkyl chains of palmitic acid on heparin was better revealed in the infrared spectrum of OPH-2 because higher degree of substitution obtained with this component as indicated in Table 1. Indeed, additional bands around 2848-2957 cm^{-1} due to the stretching

vibrations of C-H bounds of $–CH_2–$ and $–CH_3$ groups were clearly observed. Infrared absorption of OPH-2 showed three bands from 1636 cm^{-1} to 1793 cm^{-1} corresponding to carbonyl groups of the ester function. This allowed to ascertain that palmitoyl moieties are covalently bound to heparin. Whatever the synthesis method, a vibration peak around 1225 cm^{-1} was observed and was attributed to the sulfate the S=O stretches.

The synthesized *O*-palmitoyl-heparin derivatives were then used to prepare heparin nanoassemblies by mixing OPH-1 or OPH-2 with α-CD in water under moderate magnetic stirring. The association of *O*-palmitoyl-heparin and α-CD results in the formation of well-structured hexagonal-shaped nanoassemblies as showed by TEM observations (Figure 3). This kind of hexagonal shape has never been reported in the literature yet for heparin particles. Usually, spherical morphologies were obtained as reported for heparin/chitosan nanoparticles prepared by polyelectrolyte complexation [21] and deoxycholic acid-heparin amphiphilic conjugates [22].

The mechanism leading to the formation of the nanoassemblies by the auto-association of *O*-palmitoyl-heparin and α-CD is different from the one described by previous works. The explanation of the well-organized and hexagonal shape of the particles observed by TEM comes from the understanding of the mechanism of the interaction between alkyl chains and α-CD. Hexagonal crystalline structures have already been observed for short-chain compounds forming an inclusion complex of one alkyl per two α-CD [23-25]. Shaped as a hollow truncated cone, CDs are cyclic oligosaccharides of six D-(+) glucopyranose all in chair conformation. The inclusion phenomena are the result of weak interactions involving both hydrophobic and hydrophilic parts of CDs such as hydrogen bonds, electrostatic interactions and van der Waals forces. In comparison with other CDs such as β-CD and γ-CD, α-CD had the smallest cavity (4.9 Å internal diameter and 7.9 Å depth). The width of the hydrophobic part of the guest has to be lower than 4.5 Å to permit the formation of a stable inclusion compound with α-CD. This was the case of lipids such as

palmitic acid; the cross-section does not exceed 4.5 Å in the zig-zag conformation. This has been shown by the crystallographic study of the α-CD/12-dodecanoic acid complex [26]. In a more recent work, high-resolution neutron diffraction was used for the characterization of the highly hydrated α-CD/1-undecanol inclusion complex [27]. In a preceding paper, calorimetric data for the interaction of linear carboxylic acids with α-CD reported that by increasing length of the alkyl chains, the association constants increased. When the alkyl chain is not long enough (as for C6) interactions are so weak that association does not occur [28]. The interaction between palmitic acid and α-CD is thus the driving force for the formation of the nanoassemblies. A simple mixture of native heparin with α-CD in aqueous media did not give any nanoassembly formation because heparin does not form any inclusion complex with α-CD (data not shown). Hexagonal plate habitus of the crystallites seen in Figure 3 strongly suggest a molecular arrangement of the nanoassemblies in a triclinic lattice [24] in agreement with α-CD dimeric arrangement [23]. The α-CD/lipid complexes are known to crystallize spontaneously in which the hydrophobic residue of the lipid molecule is not in a disordered conformation state. This kind of interaction is typical of α-CD. It is indeed not the case of β-CD with a large ring allowing the reorientation of aliphatic chains and thus leading to higher mobility and disorder inside the host cavity [29].

The effect of *O*-palmitoyl-heparin concentration on the nanoassembly size was first studied for OPH-1. The concentration of α-CD was kept constant (10 wt%) while the concentration of the polysaccharide was progressively decreased from 1 to 0.25 wt%. At fixed concentration of α-CD, nanoassembly size increased from (344 ± 105) nm to (659 ± 260) nm when the concentration of OPH-1 was decreased from 1 to 0.25 wt% (Table 2). Furthermore, the nanoassemblies obtained at low OPH-1 concentration are highly polydisperse in comparison with the ones obtained at high OPH-1 concentration. One hypothesis to explain these results is that more than one OPH-1 is involved in nanoassembly formation.

306 The antiviral activity evaluation of nanoassemblies showed that, as expected, HSV-2 infection of
307 cells was more efficiently inhibited than that of HSV-1. The half-maximal inhibitory
308 concentrations are between 0.86 and 2.19 μg/mL against HSV-1 infection and between 0.42 and
309 1.42 μg/mL against HSV-2 infection. Previous works in the literature have also reported that
310 HSV-2 infection of cells was more efficiently inhibited that that of HSV-1 by polyanionic
311 substances such as heparin but also dextran sulphate, agar inhibitors and chondroitin sulphate B
312 [30]. Native heparin and heparin nanoassemblies did not inhibit Rotavirus infection since the cell
313 attachment and entry of Rotavirus depends on several integrins but not on HSPGs [31]. Whatever
314 the formulation, heparin nanoassemblies did not affect cell viability and the CC_{50} values were
315 higher than 300 μg/mL in all the tested cell lines indicating that the inhibitory activity does not
316 have any consequence on cytotoxicity.

317 The antiviral activity of OPH-1 was improved in comparison with heparin even without α-CD. As
318 we can see from Table 2, without α-CD the IC_{50} values against HSV-1, HSV-2 and RSV were
319 lower for OPH-1 in comparison with native heparin. The grafting of palmitic acid on the
320 hydrophilic heparin results on its hydrophobization. Previous works have reported that lipid
321 conjugates were able to increase the interaction of the molecule with biological membranes due to
322 their lipophilicity and resemblance to lipids in biological membranes [32].

323 The amphiphilic nature of OPH partly explains the higher antiviral activity obtained in comparison
324 with native heparin. The presence of α-CD will further decrease the IC_{50} for HSV-1, HSV-2 and
325 HPV-16. This increase of the antiviral activity was not due to the α-CD itself because it did not
326 have any antiviral effect (data not shown). However, the presence of α-CD leads to the formation
327 of hexagonal-shaped heparin nanoassemblies. It is likely to postulate that this hexagonal geometry
328 is favourable for the interaction of the nanoassemblies with the viruses. Previous research works

conducted on other types of nanoparticles have reported that the particle geometry influenced their interaction with cells, their subcellular trafficking and distribution in organs [33-36].

For the next experiments, the concentration of hydrophobically-modified heparin (OPH-2) was fixed at 1 wt%. The effect of α-CD concentration on nanoassembly size was investigated by progressively decreasing α-CD concentration from 10 wt% to 2.5 wt%. Table 3 depicts the physicochemical properties and shows that nanoassembly size decreased from (410 ± 24) nm to (340 ± 19) nm for α-CD concentrations of 10 wt% and 2.5 wt% respectively.

Generally speaking, the antiviral activities obtained with nanoassemblies composed of OPH-1 were better than the ones of OPH-2. There is a growing body of evidence that heparan sulphate proteoglycans act as receptors for HSV-1, HSV-2, HPV-16 and RSV. So it is expected that the antiviral activity decreased by reducing the level of sulphation. Elemental analysis of heparin and the two *O*-palmitoyl-heparin derivatives showed that the total amount of sulphur was decreased from 9.1 for heparin to 8.9 and 8.1 for OPH-1 and OPH-2 respectively (Table 1). The negative charge of heparin results from *N*-sulfation, *O*-sulfation and the presence of carboxylic groups. Particularly, *N*-sulfations and 6-*O*-sulfations of heparin play a key role in its interaction with HS-dependent viruses. The presence of sulfate groups in heparin structure results in its anticoagulant activity. Specifically, this property is due to the pentasaccharide section in heparin that has high affinity for antithrombin III. Higher sulfation of OPH-1 results in lower zeta potential of the nanoassemblies in comparison with OPH-2 (Tables 2 and 3). These differences between OPH-1 and OPH-2 nanoassemblies could be a consequence of the partial desulfation of OPH-2 in acidic medium due to hydrochloric acid release upon the reaction between palmitoyl chloride and heparin. The synthesis of OPH-1 was conducted during shorter time than for OPH-2 and in the presence of pyridine which is a basic heterocyclic organic compound. With hydrochloric acid pyridine forms a crystalline hydrochloride salt.

353 Even if the domains involved in viral binding are independent on the anticoagulant activity of
354 heparin [37], non-specific desulfation of heparin results in lower anticoagulant and antiviral
355 activities (Figure 4). So far, the anticoagulant activity of heparin is closely related to its *N*-sulfated
356 and 6-*O*-sulfated contents [37]. The desulfation of heparin at these sites decreased or even
357 abolished the antiviral activity of heparin. The sulfation of polysaccharides initially without
358 anticoagulant activity such as pullulan, allowed to obtain pullulan sulfates with potent
359 anticoagulant activity reaching the efficacy of heparin [38].

360 # 4. Conclusions

361 Novel heparin nanoassemblies active against four HSPGs-dependent viruses HSV-1, HSV-2,
362 HPV-16 and RSV were designed by a new simple and green method. The nanoassemblies were
363 formed by the auto-association of *O*-palmitoyl heparin with α-CD. Two hydrophobically-modified
364 heparins (OPH-1 and OPH-2) were obtained by using two different esterification methods.
365 Whatever the chemical method used, the observed hexagonal-shaped nanoassemblies strongly
366 suggest a crystal-like arrangement. Nanoassemblies with higher level of sulfation obtained with
367 OPH-1 exerted a stronger antiviral activity in comparison with OPH-2. These encouraging results
368 warrant further investigations of these nanoassemblies as drug delivery systems able to target the
369 HS-dependent viruses.

370 # 5. Acknowledgments

371 This work has used the facilities and the expertise of the (Electron Microscopy Platform) Cell
372 Biology unit of the Imagif platform (Centre de Recherche de Gif - www.imagif.cnrs.fr).

373 # 6. References

[1] D. Spillmann, Heparan sulfate: anchor for viral intruders? Biochimie. 83 (2001) 811- 817.

[2] J. Liu, S.C. Thorp, Cell surface heparan sulfate and its roles in assisting viral infections, Med. Res. Rev. 22 (2002) 1- 25.

[3] U. Lindahl, K. Lidholt, D. Spillmann, L. Kjellen, More to “heparin” than anticoagulation, Thromb. Res, 75 (1994) 1- 32.

[4] D.L. Rabenstein, Heparin and heparan sulfate: structure and function, Nat. Prod. Rep, 19 (2002) 312- 331.

[5] S.A. Feldman, R.M. Hendry, J.A. Beeler, Identification of a linear heparin binding domain for human respiratory syncytial virus attachment glycoprotein G. J. Virol, 73 (1999) 6610- 6617.

[6] D. WuDunn, P.G, Spear, Initial interaction of herpes simplex virus with cells is binding to heparan sulphate, J. Virol, 63 (1989) 52- 58.

[7] T. Giroglou, L. Florin, F. Schäfer, R.E. Streeck, M. Sapp, Human papilloma infection requires cell surface heparan sulfate, J. Virol, 75 (2001) 1565- 1570.

[8] M. Rusnati, E. Vicenzi, M. Donalisio, P. Oreste, S. Landolfo, D. Lembo, Sulfated K5 Escherichia coli polysaccharide derivatives: A novel class of candidate antiviral microbicides, Pharmacol. Ther, 123 (2009) 310- 322.

[9] V. Tiwari, E. Maus, I.M. Sigar, K.H. Ramsey, D. Shukla, Role of heparan sulfate in sexually transmitted infections, Glycobiology, 22 (2012) 1402- 1412.

[10] A.J. Nahmias, S. Kibrick, Inhibitory effect of heparin on herpes simplex virus, J. Bacteriol, 87 (1964) 1060- 1066.

[11] D. WuDunn, P.G. Spear, Initial interaction of herpes simplex virus with cells is binding to heparan sulphate, J. Virol, 63 (1989) 52- 58.

[12] J.G. Joyce, J-S. Tung, C.T. Przysiecji, J.C. Cook, E.D. Lehman, J.A. Sands, K.U. Jansen, P.M. Keller, The L1 major capside protein of human papillomavirus Type 11 recombinant virus-like particles interacts with heparin and cell-surface glycosaminoglycans on human keratinocytes, J. Biol. Chem, 274 (1999) 5810- 5822.

[13] K.M. Johnson, R.C. Kines, J.N. Roberts, D.R. Lowy, J.T. Schiller, P.M, Day, Role of heparan sulfate in attachment to and infection of the murine female genital tract by human papillomavirus, J. Virol, 83 (2009) 2067- 2074.

[14] Bouchemal K. Microparticles and nanoparticles made up of hydrophobized polysaccharides and alpha-cyclodextrin. WO/2013/150193A1.

[15] C.B. Buck, D.V. Pastrana, D.R. Lowy, J.T. Schiller, Efficient intracellular assembly of papillomaviral vectors, J. Virol, 78 (2004) 751- 757.

[16] M. Donalisio, M. Rusnati, V. Cagno, A. Civra, A. Bugatti, A. Giuliani, G. Pirri, M. Volante, M. Papotti, S. Landolfo, D. Lembo, Inhibition of human respiratory syncytial virus infectivity by a dendrimeric heparan sulfate-binding peptide, Antimicrob. Agents. Chemother, 56 (2012) 5278- 5288.

[17] B.S. Coulson, J.M. Tursi, W.J. McAdam, R.F. Bishop, Derivation of neutralizing monoclonal antibodies to human rotaviruses and evidence that an immunodominant neutralization site is shared between serotypes 1 and 3, Virology, 154 (1986) 302- 312.

[18] C.B. Buck, C.D. Thompson, Y.Y. Pang, D.R. Lowy, J.T. Schiller, Maturation of papillomavirus capsids, J. Virol, 79 (2005) 2839- 2846.

[19] E.P. Bianchini, J. Fazavana, V. Picard, D. Borgel, Development of a recombinant antithrombin variant as a potent antidote to fondaparinux and other heparin derivatives, Blood, 117 (2011) 2054- 2060.

[20] U. Lindahl, L. Kjellén. Heparin or heparan sulfate—what is the difference? Thromb. Haemostasis 66 (1991) 44- 48.

[21] Z.H. Liu, Y.P. Jiao, F. Liu, Z.Y. Zhang, Heparin/chitosan nanoparticle carriers prepared by polyelectrolyte complexation, J. Biomed. Mater. Res, 83A (2007) 806- 812.

[22] K. Park, K. Kim, I.C. Kwon, S.K. Kim, S. Lee, D.Y. Lee, Y. Byun, Preparation and characterization of self-assembled nanoparticles of heparin-deoxycholic acid conjugates, Langmuir, 20 (2004) 11726- 11731.

[23] C. Sicard-Roselli, B. Perly, G. Le Bas, The respective benefits of X-ray crystallography and NMR for the structural determination of the inclusion complex between butyl-isothiocyanate and alpha-cyclodextrin, J. Incl. Phenom. Macrocycl. Chem, 39 (2001) 333- 337.

[24] M. Noltemeyer, W. Saenger, Structural chemistry of linear α-cyclodextrin-polyiodide complexes. X-ray crystal structures of (α-cyclodextrin)$_2$•LiI_3•I_2•$8H_2O$ and (α-cyclodextrin)$_2$•$Cd_{0.5}$•I5•$27H_2O$. Models for the blue amylose-iodine Complex, J. Am. Chem. Soc, 102 (1980) 2710- 2722.

[25] S.S. Terdale, D.H. Dagade, K.J. Patil, Thermodynamic studies of drug-α-cyclodextrin interactions in water at 298.15 K: promazine hydrochloride/chlorpromazine hydrochloride + α-cyclodextrin + H_2O systems, J. Phys. Chem. B, 111 (2007) 13645- 13652.

[26] K. Eliadou, K. Yannakopoulou, A. Rontoyianni, I.M, Mavridis. NMR detection of simultaneous formation of [2]-and [3] pseudorotaxanes in aqueous solution between α-

cyclodextrin and linear aliphatic α, ω-amino acids, an α, ω-diamine and an α, ω-diacid of similar length, and comparison with the solid-state structures, J. Org. Chem, 64 (1999) 6217- 6226.

[27] D. Gallois-Montbrun, G. Le Bas, S.A. Mason, T. Prange, S. Lesieur, A highly hydrated-cyclodextrin/1-undecanol inclusion complex: crystal structure and hydrogen-bond network from high-resolution neutron diffraction at 20 K, Acta. Crystallogr. B, 69 (2013) 214- 227.

[28] G. Castronuovo, V. Elia, F. Velleca, G. Viscardi, Thermodynamics of the interaction of α-cyclodextrin with α,ω-dicarboxylic acids in aqueous solutions. A calorimetric study at 25°C, Thermochim. Acta, 292 (1997) 13- 37.

[29] K. Yannakopoulou, J.A. Ripmeester, I.M. Mavridis, Release of the Prays oleae pheromone as a consequence of supramolecular structure: study of the β-cyclodextrin-(Z)-tetradec-7-en-1-al complex by X-ray crystallography and NMR spectroscopy in the solid state and in solution, J. Chem. Soc. Perkin Trans. 2, 2 (2002) 1639- 1644.

[30] R.D. Hutton, D.L. Ewert, G.R. French, Differentiation of types 1 and 2 of herpes simplex virus by plaque inhibition with sulfated polyanions, Proc. Soc. Exp. Biol. Med, 142 (1973) 27- 29.

[31] S. López, C.F. Arias, Multistep entry of rotavirus into cells: a Versaillesque dance, Trends. Microbiol, 12 (2004) 271- 278.

[32] F. Castelli, G. Giammona, A. Raudino, G, Puglisi. Macromolecular prodrugs interaction with mixed lipid membrane. A calorimetric study of naproxen linked to polyaspartamide interacting with phosphatidylcholine and phosphatidylcholine-phosphatidic acid vesicles, Int. J. Pharm, 70 (1991) 43- 52.

[33] J.A. Champion, Y.K. Katare, S. Mitragotri, Particle shape: a new design parameter for micro- and nanoscale drug delivery carriers, J. Control. Release, 121 (2007) 3- 9.

[34] B.D. Chithrani, A.A. Ghazani, W.C.W. Chan, Determining the size and shape dependence of gold nanoparticle uptake into mammalian cells, Nano. Lett, 6 (2006) 662- 668.

[35] M. Ornatska, S. Peleshanko, K.L. Genson, B. Rybak, K.N. Bergman, V.V. Tsukruk, Assembling of amphiphilic highly branched molecules in supramolecular nanofibers, J. Am. Chem. Soc, 126 (2004) 9675- 9684.

[36] O. Cauchois, F. Segura-Sanchez, G. Ponchel, Molecular weight controls the elongation of oblate-shaped degradable poly (γ-benzyl-l-glutamate) nanoparticles, Int. J. Pharm, 452 (2013) 292- 299.

[37] B.C. Herold, S.I. Gerber, T. Polonsky, B.J. Belval, P.N. Shaklee, K. Holme, Identification of structural features of heparin required for inhibition of herpes simplex virus type 1 binding, Virology, 206 (1995) 1108- 1116.

471 [38] S. Alban, A. Schauerte, G. Franz, Anticoagulant sulfated polysaccharides Part I Synthesis and
472 structure-activity relationships of new pullulan sulfates, Carbohyd Polym, 47 (2002) 267- 276.

Figure caption:

Figure 1. Synthetic scheme of the two methods for the grafting of palmitic acid on heparin.

Figure 2. ATR-IR spectra of OPH-1 and OPH-2 and comparison with native heparin.

Figure 3. TEM observations of Hep2 **(A)** and Hep6 **(B)**.

Figure 4. Anticoagulant activity of heparin nanoassemblies Hep2 and Hep6 composed of 1 wt% of OPH-1 and OPH-2 respectively and 10 wt% of α-CD. The results were compared to the anticoagulant activity of native heparin. The anticoagulant activity was expressed by U/mg of heparin or *O*-palmitoyl-heparin.

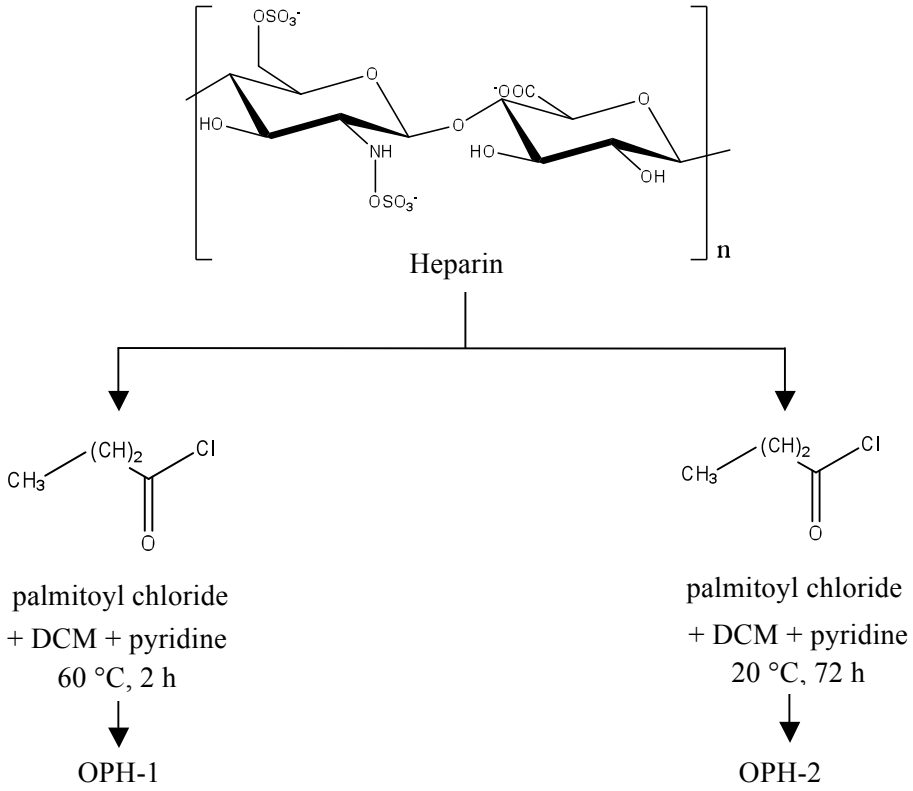
OSO3-
O
HO
NH
OSO3-
O
-OOC
O
HO
OH
n
Heparin
CH3
(CH)2
Cl
O
palmitoyl chloride
+ DCM + pyridine
60 °C, 2 h
OPH-1
CH3
(CH)2
Cl
O
palmitoyl chloride
+ DCM + pyridine
20 °C, 72 h
OPH-2

Figure 1:

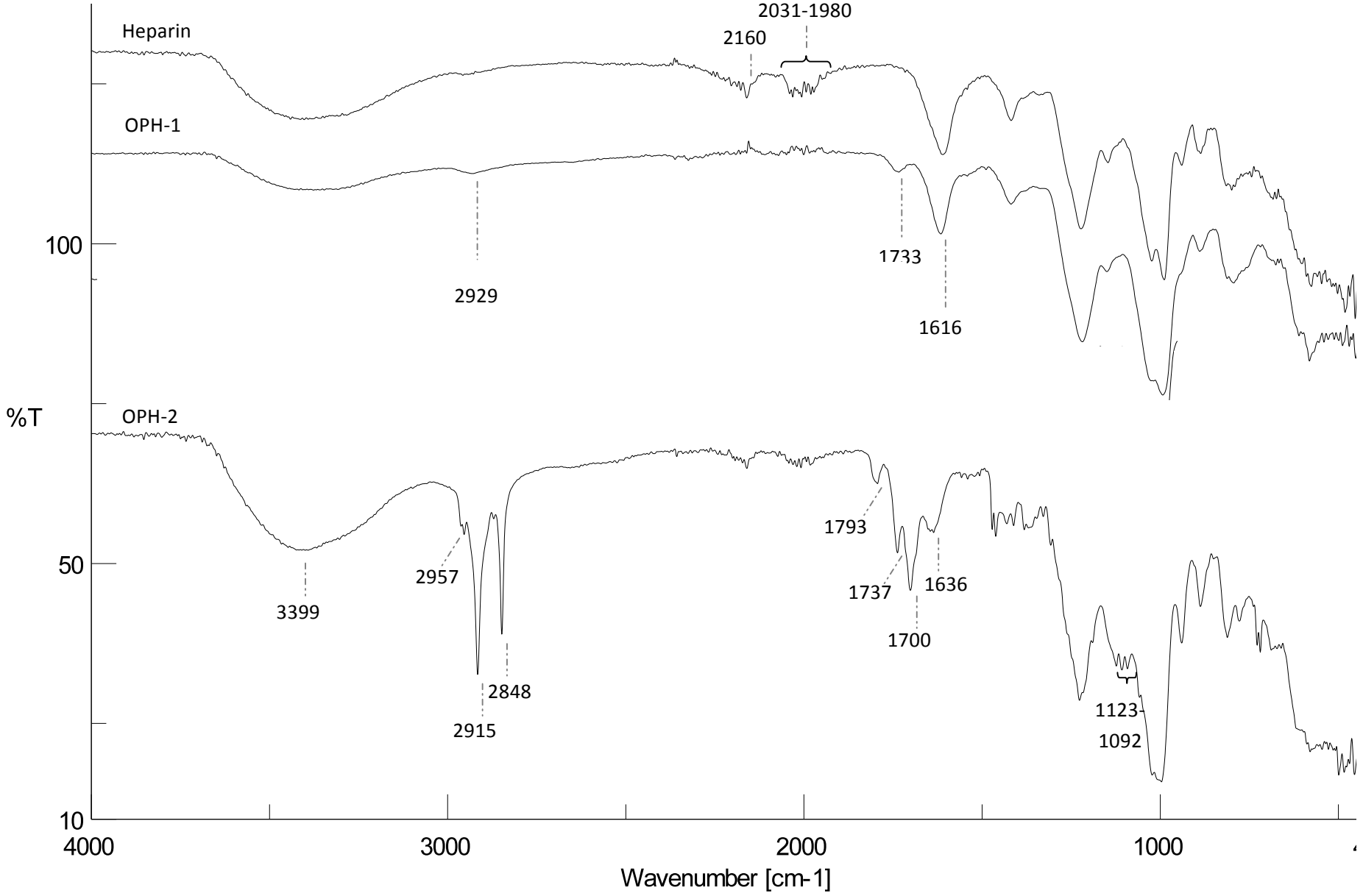
Heparin
2031-1980
2160
OPH-1
100
2929
1733
1616
%T
OPH-2
50
3399
2957
1793
1737
1636
1700
2848
2915
1123
1092
10
4000
3000
2000
1000
Wavenumber [cm-1]

1

Figure 2.

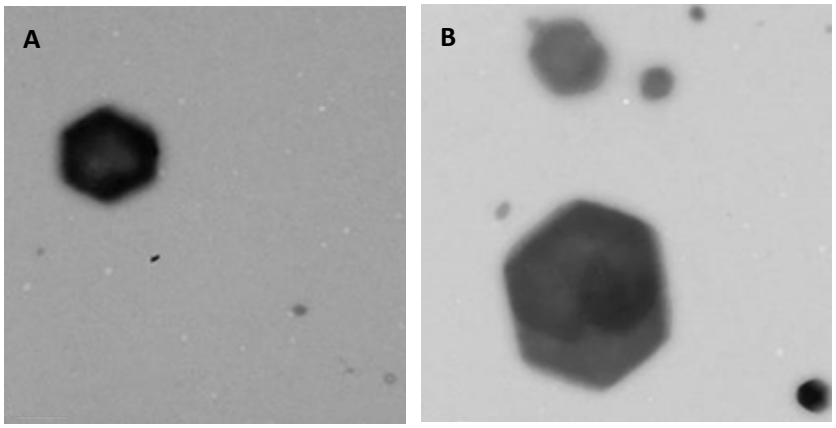

Figure 3.

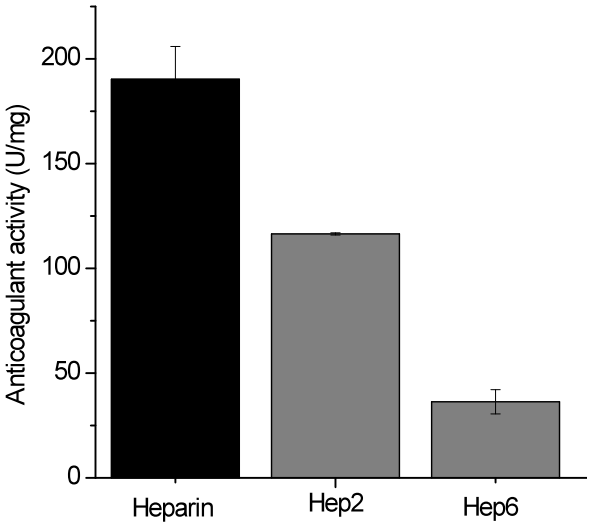
Anticoagulant activity (U/mg)
200
150
100
50
0
Heparin
Hep2
Hep6

Figure 4.

Table 1: Total carbon and sulfur quantification evaluated by elemental analysis into *O*-palmitoyl-heparins (OPH-1 and OPH-2) in comparison with native heparin.

Polymer	**Total C in OPH (% w/w)**	**Total C in OPH (% mol)[a]**	**DS[b] (%)**	**Total S in OPH (% w/w)**
Heparin	19.0	3.1	-	9.1
OPH-1	21.8	3.6	0.5	8.9
OPH-2	33.7	5.6	2.5	8.1

[a]Total carbon in OPH conjugates was calculated from the equation C%6

[b]The degree of substitution was calculated from the equation Eq.1.

Table 2. Effect of OPH-1 concentration on assembly D_h and their antiviral activities against HSV-1, HSV-2, HPV16-SEAP PsV and RSV. The content of α-CD was kept constant, while OPH-1 was progressively decreased from 1 to 0.25 wt%. Rotavirus was used as a control. Polydispersity indexes were lower than 0.10, indicating a relatively homogenous size distribution.

Polymer	Assembly code	OPH-1 (wt%)	α-CD (wt%)	D_h (nm)	ξ (mV)	virus	IC_{50} µg/mL (95% C.I.)	CC_{50} (µg/mL)	SI
Heparin	-	-	-	-	-	HSV-1	2.19 (0.97 - 3.56)	> 300	> 136.98
						HSV-2	1.42 (0.23 - 2.55)	> 300	> 211.26
						HPV-16	2.01 (1.12 - 3.88)	> 300	> 149.25
						RSV	2.11 (1.69 - 3.43)	> 300	> 142.18
						Rotavirus	-[b]	> 300	
OPH-1	**Hep1**	1	0	-[a]		HSV-1	1.62 (0.51- 2.66)	> 300	> 185.18
						HSV-2	0.62 (0.13 - 1.78)	> 300	> 483.87
						HPV-16	2.88 (1.81 - 4.21)	> 300	> 104.16
						RSV	0.94 (0.47 - 1.87)	> 300	> 319.14
						Rotavirus	-[b]	> 300	
	Hep2	1	10	344 ± 105	-59 ± 1	HSV-1	1.07 (0.13 - 2.07)	> 300	> 280.37
						HSV-2	0.51 (0.08 - 1.92)	> 300	> 588.23
						HPV-16	1.25 (0.33 - 2.04)	> 300	> 240.00
						RSV	1.00 (0.46 - 2.17)	> 300	> 300.00
						Rotavirus	-[b]	> 300	
	Hep3	0.5	10	344 ± 128	-58 ± 1	HSV-1	0.99 (0.21- 1.99)	> 300	> 303.03
						HSV-2	0.66 (0.09 - 2.10)	> 300	> 454.54
						HPV-16	1.76 (0.69 - 4.11)	> 300	> 170.45
						RSV	0.99 (0.47 - 2.10)	> 300	> 303.03
						Rotavirus	-[b]	> 300	
	Hep4	0.25	10	659 ± 260	-62 ± 2	HSV-1	0.86 (0.32 - 2.05)	> 300	> 348.83
						HSV-2	0.42 (0.24 - 1.68)	> 300	> 714.28
						HPV-16	2.20 (1.03 - 5.43)	> 300	> 136.36
						RSV	1.01 (0.51 - 1.99)	> 300	> 297.02
						Rotavirus	-[b]	> 300	

[a] -, no formation of the assemblies.

[b] -, the compound was non inhibitory at a dose of ≤ 100 µg/mL.

Table 3. Effect of α-CD concentration on assembly D_h and their antiviral activities against HSV-1, HSV-2, HPV16-SEAP PsV and RSV. The concentration of OPH-2 was kept constant, while α-CD concentration was progressively decreased from 10 wt% to 2.5 wt%. Rotavirus was used as a negative control. Polydispersity indexes were lower than 0.10, indicating a relatively homogenous size distribution.

Polymer	Assembly code	OPH-1 (wt%)	α-CD (wt%)	D_h (nm)	ξ (mV)	virus	IC_{50} μg/mL (95% C.I.)	CC_{50} μg/mL	SI
Heparin	-	-				HSV-1	2.19 (0.97 - 3.56)	> 300	> 136.98
						HSV-2	1.42 (0.23 - 2.55)	> 300	> 211.26
						HPV-16	2.01 (1.12 - 3.88)	> 300	> 149.25
						RSV	2.11 (1.69 - 3.43)	> 300	> 142.18
						Rotavirus	-	> 300	
OPH-2	**Hep6**	1	10	340 ± 19	-52 ± 1	HSV-1	5.55 (3.27- 10.34)	> 300	> 54.05
						HSV-2	2.52 (1.06 - 6.59)	> 300	> 119.04
						HPV-16	n.c.[a]	> 300	
						RSV	5.41 (2.83 - 10.33)	> 300	> 55.45
						Rotavirus	-[b]	> 300	
	Hep7	1	5	355 ± 11	-53 ± 1	HSV-1	4.09 (2.89 - 9.27)	> 300	> 73.34
						HSV-2	2.39 (0.41 - 8.03)	> 300	> 125.52
						HPV-16	n.c.	> 300	
						RSV	2.45 (1.59 - 3.78)	> 300	> 122.44
						Rotavirus	-	> 300	
	Hep8	1	2.5	410 ± 24	-54 ± 4	HSV-1	5.03 (2.54 - 8.29)	> 300	> 59.64
						HSV-2	2.54 (1.31 - 4.81)	> 300	> 118.11
						HPV-16	2.50 (1.33 - 3.46)	> 300	> 120.00
						RSV	1.15 (0.65 - 2.04)	> 300	> 260.86
						Rotavirus	-	> 300	

[a] n.c., not calculable.

[b] -, the compound was non inhibitory at a dose of ≤ 100 μg/mL.